Clim Dyn (2017) 48:2153–2172
DOI 10.1007/s00382-016-3197-1

Finding the driver of local ocean–atmosphere coupling in reanalyses and CMIP5 climate models

Alfredo Ruiz-Barradas[1] · Eugenia Kalnay[1,2] · Malaquías Peña[3] · Amir E. BozorgMagham[4] · Safa Motesharrei[2,5,6]

Received: 17 September 2015 / Accepted: 20 May 2016 / Published online: 7 June 2016

Abstract Identification of the driver of coupled anomalies in the climate system is of great importance for a better understanding of the system and for its use in predictive efforts with climate models. The present analysis examines the robustness of a physical method proposed three decades ago to identify coupled anomalies as of atmospheric or oceanic origin by analyzing 850 mb vorticity and sea surface temperature anomalies. The method is then used as a metric to assess the coupling in climate simulations and a 30-year hindcast from models of the CMIP5 project. Analysis of the frequency of coupled anomalies exceeding one standard deviation from uncoupled NCEP/NCAR and ERA-Interim and partially coupled CFSR reanalyses shows robustness in the main results: anomalies of oceanic origin arise inside the deep tropics and those of atmospheric origin outside of the tropics. Coupled anomalies occupy similar regions in the global oceans independently of the spatiotemporal resolution. Exclusion of phenomena like ENSO, NAO, or AMO has regional effects on the distribution and origin of coupled anomalies; the absence of ENSO decreases anomalies of oceanic origin and favors those of atmospheric origin. Coupled model simulations in general agree with the distribution of anomalies of atmospheric and oceanic origin from reanalyses. However, the lack of the feedback from the atmosphere to the ocean in the AMIP simulations reduces substantially the number of coupled anomalies of atmospheric origin and artificially increases it in the tropics while the number of those of oceanic origin outside the tropics is also augmented. Analysis of a single available 30-year hindcast surprisingly indicates that coupled anomalies are more similar to AMIP than to coupled simulations. Differences in the frequency of coupled anomalies between the AMIP simulations and the uncoupled reanalyses, and similarities between the uncoupled and partially coupled reanalyses, support the notion that the nature of the coupling between the ocean and the atmosphere is transmitted into the reanalyses via the assimilation of observations.

Keywords Ocean–atmosphere coupling · Coupled anomalies · Driver of coupled anomalies · SST · Vorticty · CMIP5

✉ Alfredo Ruiz-Barradas
aruizb@umd.edu

1 Department of Atmospheric and Oceanic Science, University of Maryland, 3435 Computer and Space Science Building, College Park, MD 20742-2425, USA

2 The Institute of Physical Science and Technology, University of Maryland, College Park, MD, USA

3 IMSG at EMC/NCEP/National Weather Service, College Park, MD, USA

4 Northern Virginia Community College, Loudoun, VA, USA

5 Department of Physics, University of Maryland, College Park, MD, USA

6 National Socio-Environmental Synthesis Center, Annapolis, MD, USA

1 Introduction

The oceans and atmosphere form a coupled system that exchanges heat, momentum, and water at the air–sea interface. Understanding these interactions is fundamental to realistically simulate climate variability and change. Climate and its variability are strongly influenced by the ocean and in particular the sea surface temperatures (SSTs). As such, SSTs are a source for potential predictability for climate fluctuations. The large-scale structure of the SST anomalies depends not only on large-scale atmospheric circulation and ensuing energy fluxes but also on heat transport by currents and vertical mixing (Ekman currents and pumping) as well as boundary layer depth (Deser et al. 2010). The coupling between SST anomalies and the overlaying atmospheric circulation varies geographically. For example, it has been shown that the extra-tropical atmospheric circulation variability, which is intrinsic to the atmosphere, produces large-scale SST anomalies (e.g. Bryan and Stouffer 1991). However it has also been shown that large-scale atmospheric variability in the tropics is largely the result of oceanic processes (Deser et al. 2010). The misrepresentation of the forcing from the atmosphere to the ocean, or its omission as takes place in the type of simulations known as the Atmospheric Model Intercomparison Project (AMIP, Gates 1992), in which the atmosphere is influenced by observed SSTs but cannot change them, has important implications. Without accounting for this feedback from the atmosphere to the ocean, the thermal variance in both the ocean and the atmosphere is reduced (e.g., Barsugli and Battisti 1998) as is the predictability skill in the midlatitudes' atmosphere as a result of short-lived anomalies (Peña et al. 2004). In turn, a deficient representation of the coupling from the ocean to the atmosphere would result in a poor simulation of large scale climate variability in the tropics (Mo and Kalnay 1991). Thus it is clear that the ocean state and atmospheric circulation cannot be treated independently of each other without feedbacks.

The interactions between the ocean and atmosphere and their feedbacks help to define the climate and its variability. These interactions and feedbacks are largely related to changes in surface winds, surface evaporation, sea surface temperatures, atmospheric convection, cloud cover and ocean dynamics. The feedbacks belong to two main categories: (1) the purely dynamical Bjerknes feedback relating surface winds to dynamical ocean adjustments (Bjerknes 1969), and (2) the thermodynamic feedbacks such as the wind-evaporation-SSTs (or WES: Xie and Philander 1994) and the cloud/water vapor—SST involving surface heat fluxes. Under the Bjerknes feedback an easterly wind anomaly along the equatorial ocean induces Ekman upwelling of cold water to the surface over the shallow mixed layer in the eastern portion of the domain; the upwelling of cold subsurface waters provokes an upward tilt of the thermocline, cools the ocean and suppresses convection over the eastern equatorial ocean which in turn helps to maintain the surface pressure gradient needed to sustain the easterly wind anomalies. Under the WES feedback on the other hand, a positive SST anomaly under easterly trade winds will induce a surface low pressure with westerly anomaly winds to its south and easterly anomaly winds to its north which will enhance the easterly trade winds to its north and will decrease them to the south of the initial positive SST anomaly. The increased trade winds to the north will cool down the SSTs by increasing latent heat flux while the decreased trade winds to the south will warm up the SSTs by decreasing the latent heat flux causing the initial positive SST anomaly to move to the south. In the case of a positive and negative SST dipole to the north and south of the equator, the WES feedback works to enhance the initial dipole. While the Bjerknes feedback can be seen operating zonally along the equatorial oceans, the WES feedback operates not only within the equatorial and tropical oceans but outside of them. While these feedbacks are often invoked to explain the ocean–atmosphere coupling within the tropics, their roles over the extratropics have been minimized, although not completely rejected, especially due to the lack of a strong relationship between local surface winds and SSTs to oceanic conditions. Instead, the ocean is seen as an integrator of the atmospheric synoptic weather over the extratropics responding sometime remotely to a tropical forcing or to changes in the gyre and thermohaline circulations. The present paper does not attempt to review the ocean–atmosphere interactions, but rather to use these local feedback mechanisms for context through which to examine the nature of the coupling. The paper by Wang et al. (2004) provides to the reader with a more detailed overview of ocean–atmosphere interactions.

Interactions between the ocean and the atmosphere are complex and occur on a wide range of spatial and temporal scales. Both observations and models are important tools to identify and understand these interactions. With the development of reanalyses and coupled climate models it is becoming possible to not only assess the nature of these interactions but also assess to what degree these interactions are present in observations, their realism in models, and the ways the couplings can be identified. Lead/lag correlation between SSTs and atmospheric variables have been used previously to examine the origin of locally coupled anomalies (e.g., Peña et al. 2003; Kumar et al. 2013). Most notably, lead/lag correlations between SSTs and rainfall in the central Pacific allowed Kumar et al. (2013) to conclude that the nature of the coupling between the ocean and the atmosphere in this region is transmitted to the atmosphere via the assimilation of observed data in uncoupled reanalyses. In addition to reanalyses, it is also known that climate models display distinct behavior regarding the role of ocean–atmosphere interactions in generating climate variability. These models have ocean–atmosphere interactions that allow them, with different degrees of accuracy, to simulate large-scale climate variability in the tropics (like ENSO—e.g. Bellenger et al. 2014), as well as extra-tropical climate variability, which do not owe their existence to two-way ocean–atmosphere interactions (like the North Atlantic Oscillation, NAO—e.g. Davini and Cagnazzo 2013). However, there is not a consistent way to identify and assess the direction of the forcing-response relationship or the nature of the ocean–atmosphere coupling (as it will be referred to) in the current state-of-the-art global coupled models used in climate variability and change studies.

A simple and physically based method to identify the nature of the coupling between the atmosphere and the ocean was introduced by Kalnay et al. (1986) and later used by Mo and Kalnay (1991) and Peña et al. (2003). The method arose as coupled anomalies were identified in observations of the Pacific Ocean (Kalnay et al. 1986; Mo and Kalnay 1991). This method identifies the driver in the local coupling by checking whether a cyclonic vorticity anomaly is located above a cold ocean anomaly or above a warm ocean anomaly and is displayed schematically in Fig. 1 when horizontal advection is neglected as it is in this study; Mo et al. (1987) and Peña et al. (2003) showed how this method can be modified in order to include horizontal advection.

If the atmosphere drives the ocean (Fig. 1, top panels), a cyclonic atmospheric anomaly will induce divergence of the surface waters and upwelling of cold subsurface temperature anomalies in the oceanic mixed layer driven by Ekman pumping. This circulation is associated with cloudy skies that reduce insolation of the surface and cool the ocean surface further. Conversely, an anti-cyclonic circulation anomaly will induce convergence of surface waters and downwelling of warm SST anomalies in the oceanic mixed layer. This circulation is associated with clear skies that enhance insolation and warming of the ocean surface. These processes are similar to the initial setting of the anomalies in the Bjerknes feedback theory when surface

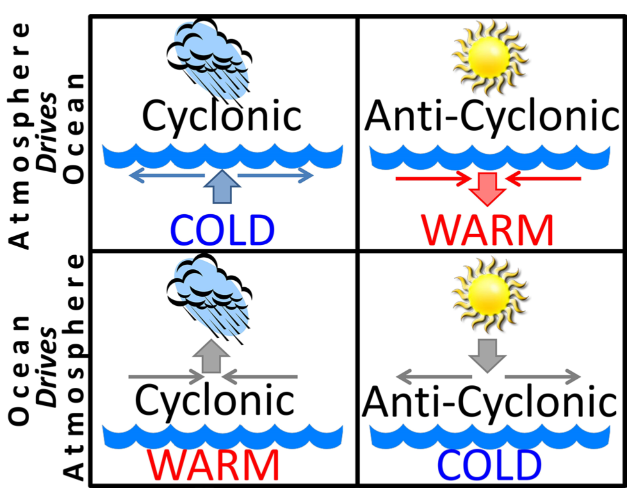

Fig. 1 Schematic diagram illustrating the proposed metric of the local dynamical ocean–atmosphere coupling assuming there is no horizontal advection. *Upper panels* show the cases when the atmospheric circulation drives the ocean while *lower panels* show the cases when the surface temperatures of the ocean drive the atmospheric circulation. It shows the relationship between slowly varying sea surface temperature anomalies and low-level atmospheric vorticity anomalies. Adapted from Mo and Kalnay (1991)

wind anomalies drive SST anomalies due to Ekman pumping. In this case where the atmosphere is forcing the ocean, the associated atmospheric conditions (cloudy vs. sunny) deepen the surface temperature anomalies forced by the anomalous circulation. In this way the atmospheric conditions provide a negative feedback to the atmospheric circulation driver since these conditions at the surface tend to induce the reverse circulations in the atmosphere.

On the other hand, when the ocean drives the atmosphere (Fig. 1, bottom panels) warm ocean anomalies will drive upward motion in the lower atmosphere by creating a low pressure zone, low-level convergence, a cyclonic circulation and cloud development. Cold ocean anomalies will oppositely drive downward motion in the lower atmosphere by creating a high pressure zone, low-level divergence, an anti-cyclonic circulation and clear skies. This is similar to the WES feedback setting of the anomalies when the release of latent heat promotes surface divergence or convergence and the corresponding low level circulation. In this case when the ocean is forcing the atmosphere, the associated atmospheric conditions (cloudy vs. sunny) enhance the anomalous circulation initially forced by the anomalous ocean surface conditions. However, the atmospheric conditions also provide a negative feedback to the ocean surface as they induce the reverse ocean surface temperature anomalies. Thus, it is apparent that *the feedback from the atmospheric conditions (cloudy vs. sunny) in the coupled anomalies of both atmospheric and oceanic origin tends to weaken the driver of the anomaly and strengthen the driven anomaly*.

The main goals of the present analysis are (1) to extend the assessment made by Peña et al. (2003) of the robustness of this driver rule through the analysis of several different reanalyses and AMIP-style simulations, and (2) to assess the nature of the local ocean–atmosphere coupling in the climate and Earth system models that participated in phase 5 of the Coupled Model Intercomparison Project (CMIP5, Taylor et al. 2011). The set of models from the CMIP5 project provides a unique opportunity to contrast the statistics of coupled anomalies in both two and one-way interaction models, since fully coupled, AMIP-type simulations, and decadal predictions were carried out with the same models. The metric proposed by Kalnay et al. (1986) for identification of the driver of the coupled ocean–atmosphere anomalies could be a valuable tool not only to assess the degree of coupling in the state-of-the-art models (that are being used for climate variability and change projections) but also to diagnose the effect on the coupling of the atmospheric feedback on the ocean that is absent in the AMIP simulations and the extent of the 2-way coupling in decadal climate predictions. This metric is easy to calculate, reproduce and interpret, and can be applied to both the mean climate and climate variability providing a useful complement to other in-depth diagnosis tools. Similar results to those presented here have been obtained by BorzogMagham et al. (Manuscript in preparation) who applied the Granger causality theory to the same set of variables in order to statistically determine the driver of ocean–atmosphere coupled anomalies. Since the Granger causality theory is based on statistical information theory and does not require any a priori physical phase relationship between the variables the agreement of their results strongly supports the validity of the physical phase relationship shown in Fig. 1 to determine the driver.

The paper is organized as follows. Section 2 presents the datasets and models used and the method used to identify the nature (i.e., direction) of the coupling. Section 3 analyzes the coupling in several observationally based products and assesses the robustness of the results. Section 4 analyzes the coupling in the simulations of the twentieth century climate from a selected group of models participating in the CMIP5 project, and in the available decadal hindcast. Section 5 presents a summary and conclusions of the paper.

2 Data sets and methodology

The present analysis uses SSTs and 850 mb vorticity at several temporal resolutions from observations, reanalyses, and simulations of the twentieth century climate and a single 30-year hindcast from models participating in the CMIP5 project of the Intergovernmental Panel on Climate Change (IPCC 2013).

2.1 Observations and reanalyses

Observed SST datasets come from two different sources: the monthly U.K. Met Office's Hadley Centre Sea Ice and Sea Surface Temperature dataset, version 1.1 (HadISST1.1, Rayner et al. 2003), and NOAA's daily Reynolds Optimum Interpolation Sea Surface Temperature Analysis, version 2 (OIv2 SSTs, Reynolds et al. 2002). Three reanalyses products are used: the first generation NCEP/NCAR reanalysis (Kalnay et al. 1996), the third generation reanalyses such as NCEP's Climate Forecast System Reanalysis (CFSR—Saha et al. 2010), and the European Centre for Medium-Range Weather Forecasting's Atmospheric reanalysis (ERA-Interim—Dee et al. 2011). In the NCEP/NCAR and ERA-Interim reanalyses global observed SSTs and sea–ice concentrations from several sources are used as boundary conditions for the atmospheric forecast model. In this way, these two reanalysis products of the atmospheric fields are done in an uncoupled mode. In the CFSR, on the other hand, the SST predicted by the ocean data assimilation model is relaxed towards the observed SSTs every 6 h to one-fourth of the daily analyzed value. In this other product, the reanalysis of the atmospheric fields is done in a weakly coupled data assimilation mode in which the analysis of oceanic and atmospheric components are done separately, while the 6-h guess forecast is made based on a coupled model. In the reanalyses products some of the forecasted atmospheric variables are updated with observed values in the assimilation process. Monthly resolution data were obtained from all these reanalyses but daily data were only obtained from NCEP/NCAR reanalysis.

2.2 CMIP5 models and experiments

The CMIP5 model simulations of the twentieth century climate analyzed here are of two types: *historical* and *AMIP*. The *historical* simulations come from fully coupled ocean–atmosphere climate models. The *AMIP* simulations, on the other hand, come from atmospheric models used in the historical simulations that were forced with observed SSTs. In both cases simulations are run by imposing observed changing atmospheric composition (due to both anthropogenic and volcanic influences), solar forcing, emissions or concentrations of short-lived species as well as natural and anthropogenic aerosols and land use change. The historical simulations are usually started from multi-century preindustrial control (quasi equilibrium) integrations starting around 1860. In addition, a 30-year hindcast initialized from a climate state in 1980 is analyzed (Taylor et al. 2011; Yeager et al. 2012).

Consistency between the SSTs and atmospheric conditions in model simulations can be important for a proper capture of the air–sea coupling as different SSTs could get different atmospheric responses. On this regard, forcing atmospheric models with SSTs generated by the same coupled model can provide that consistency not present in the AMIP simulations forced with observed SSTs (e.g. Zhu and Shukla 2013) however these types of simulations are not available from the CMIP5 pool of simulations. Thus AMIP-style simulations are used as they provide the extreme case where the atmospheric coupling has been eliminated and the observed SST forcing is common to all models. In contrast the 30-year hindcast is a fully coupled experiment initialized with an initial condition of the ocean on January 1, 1980. Integration is done through the whole 30 year period under observed atmospheric composition (and other conditions including volcanic aerosols) prescribed as in the historical simulations. The initial condition is obtained from a forced ocean–sea ice simulation designed to reproduce the observed evolution of the ocean and sea ice states for the period 1948–2007 (Yeager et al. 2012). This 30-year hindcast is challenging as it lies between the subseasonal-to-interannual scale and the centennial prediction scale, which differ in their reliance on either the initial conditions or boundary conditions, respectively, for a successful prediction. At this time scale of the hindcast, it is expected that the external forcing from increasing greenhouse gases might dominate the response. However, it is possible some residual influence from the initial conditions might still be detectable.

The CMIP5 models analyzed include: (1) version 4 of the NCAR's Community Climate System Model CCSM4 (Gent et al. 2011), (2) version 3 of the NOAA's GFDL Coupled Climate Model GFDL-CM3 (Donner et al. 2011; Griffies et al. 2011), (3) UKMO Hadley Centre Global Environment Model version 2, in its Earth System configuration, UKMO-HadGEM2-ES (Collins et al. 2008; Martin et al. 2011), and (4) Germany's version 6 of the European Centre Hamburg Model/MPI-M's Earth System Model, Low Resolution version, ECHAM6/MPI-ESM-LR (Raddatz et al. 2007; Marsland et al. 2003). It is important to note that the CMIP5 versions of the models from NCAR and GFDL are updated versions of the CMIP3 models, but the CMIP5 versions of the models from UKMO and MPI are Earth System models which in addition to the atmosphere, ocean, land and sea ice model components also include the carbon cycle in the land, atmosphere and ocean components. Since no AMIP simulation was available from the UKMO-HadGEM2-ES model, the UKMO-HadGEM2-A model (Collins et al. 2008; Martin et al. 2011) was used instead. The only hindcast available for the analysis comes from the CCSM4 model.

The historical twentieth century climate simulations started from the mid nineteenth century and finished in 2004 or 2005 depending on the model, but unlike the CMIP3 simulations (Meehl et al. 2007), the forcing was standardized for all models. On the other hand the AMIP-style simulations started in 1979 and finished in 2008 or 2010 depending on the model. All simulations come from their corresponding ensemble member one, while the hindcast is from ensemble member ten.

Differences between the analyzed model simulations and reanalyses are clear and are summarized in Table 1.

2.3 The metric

The results of the method presented in this paper are computed largely at monthly resolution but a comparison is also made using data at daily and pentad (5-day means) resolutions. Data at daily and pentad resolutions needed to be preprocessed in order to make all years the same length to avoid the extra day in leap years. The extra day in a leap year was averaged with the previous day (28 of February) in order to have 365-day years, while the same extra day was added to the average of the 12th pentad (25 February-1 March—a sextet now) in order to have 73-pentad years. The method uses anomalies that are obtained differently according to the temporal resolution. Following Peña et al. (2003) monthly resolution anomalies are obtained by subtracting the long-term mean climatology of the field, but anomalies at daily and pentad resolutions are obtained after subtracting the first and second harmonics (i.e., annual and semi-annual cycles) of the field at each resolution (Wang et al. 2009). Results presented at daily and pentad resolutions barely change if anomalies are calculated with respect to the daily and pentad long-term climatologies. Monthly anomalies are calculated with respect to the common period 1979–2004 unless stated otherwise; daily and pentad anomalies are calculated with respect to the first and second harmonics of the period 1982–2013. These anomalies are then compared against their corresponding all-year standard deviation (around the monthly, pentad, and daily means) and o*nly those whose amplitude exceeds one standard deviation are considered when counting the frequency of the coupled anomalies*. This approach differs from Peña et al. (2003) where anomalies were smoothed and compared against a fraction of the standard deviation of the original raw anomalies. The significance of the results when applying the proposed metric for the analysis of the local coupled anomalies arises from the fact that anomalies are larger than one standard deviation.

The use of this method over a grid point in the tropical Pacific is shown in Fig. 2 when SST and 850 mb vorticity

Table 1 Differences between analyzed model simulations, hindcast and reanalyses

Historical simulations and Hindcast	CFSR reanalysis	AMIP simulations	NCEP/NCAR and ERA-interim reanalyses
Fully Coupled ocean–atmosphere models	Weak Coupling from relaxing forecasted SSTs to observed SSTs Some forecasted atmospheric variables are updated with observed values	Atmosphere model forced with observed SSTs	Atmosphere model with observed sea–ice & SSTs as boundary conditions Some forecasted atmospheric variables are updated with observed values
Two-way ocean–atmosphere interactions	Weak two-way ocean–atmosphere interactions	One-way interactions from the ocean to the atmosphere	One-way interactions from the ocean to the atmosphere

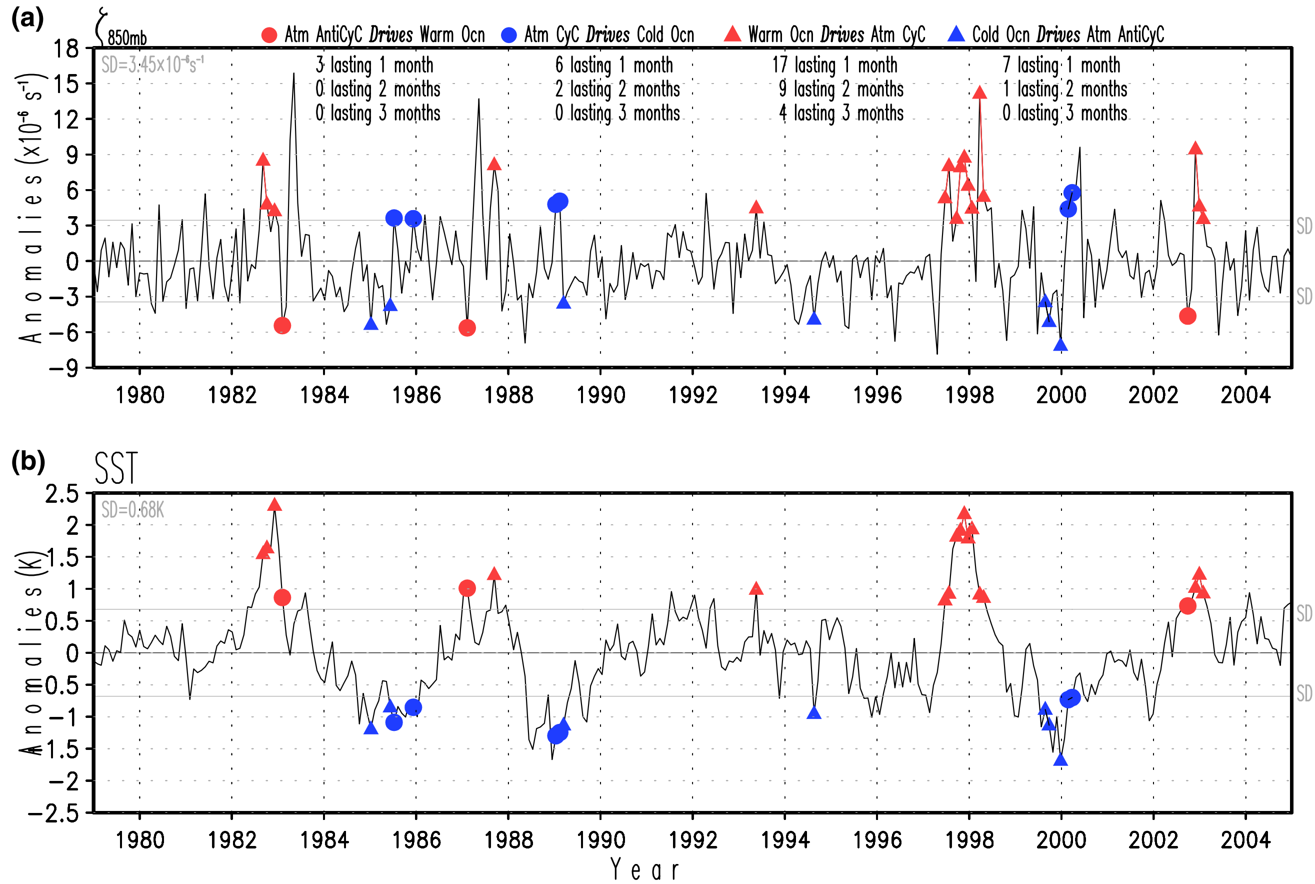

Fig. 2 Identification of the frequency of coupled ocean–atmosphere anomalies following the dynamic criteria at 120°W, 5.25°N over the tropical Pacific from monthly time series of the Climate Forecast System Reanalysis (CFSR) for the period 1979–2004. Panels show time series of **a** vorticity anomalies at 850 mb ($\zeta_{850\ \mathrm{mb}}$), and **b** SST anomalies; anomalies are with respect to the 1979–2004 climatology. The metric is applied only for anomalies exceeding one standard deviation (*thin horizontal gray lines*). Anomalies where the atmosphere drives the ocean are identified by the *filled circles*, while those where the ocean drives the atmosphere are marked by *filled triangles*. *Red/blue circles* indicate that an anti-cyclonic/cyclonic circulation in the atmosphere drives warm/cold SST anomalies in 3/6 months; only 2 of the cyclonic-cold SST coupled anomalies last 2 months. *Red/blue triangles* indicate that warm/cold SST anomalies drive a cyclonic/anti-cyclonic circulation in 17/7 months; 9 of the warm SST-cyclonic coupled anomalies last 2 months, and 4 of them last 3 months but only 1 of the cold SST-anti-cyclonic coupled anomalies last 2 months

anomalies exceed their corresponding one standard deviation. The metric identifies 9 cases where the atmosphere forces the ocean (circles) and 24 where the ocean forces the atmosphere (triangles). From these cases, only 2 of the coupled anomalies forced by the atmosphere persist for 2 months and none for 3 months; on the other hand, 10 of the coupled anomalies forced by the ocean persist for 2 months, and 4 persist for three consecutive months (see the figure caption for further details about the partitioning of the different cases). Similar results are obtained when using ERA-Interim and other observationally-based products (not shown). This metric for identification of the driver in coupled anomalies can be used to display on a map the regions where one forcing is more dominant than the other at several temporal scales from daily to monthly. The following analysis will be focused on monthly anomalies unless specified otherwise.

The method is applied in the context explained and outlined in Fig. 1 and it does not attempt to be inclusive of all types of coupling as explained in the Introduction. For instance, the large scale atmospheric circulation forcing of SST anomalies along the coasts is not identified by the present method. In fact, it would be wrongly classified as a coupled anomaly of oceanic origin as it looks for the local relationship between the fields. The proposed method captures coupled anomalies generated when the Bjerknes and the WES feedbacks are acting. The former is active for the coupled anomalies of atmospheric origin, and the latter for those anomalies of oceanic origin.

3 Nature of the coupling in different reanalyses products

The nature of the global ocean–atmosphere coupling is investigated in this section. This is done by analyzing the metric from several reanalyses products to ensure robustness (Fig. 3).

3.1 Similarities in the coupling from different coupling schemes

Similarities among the different reanalyses are striking in spite of their differences in SSTs, horizontal resolutions, and the uncoupled nature of NCEP/NCAR and ERA-Interim reanalyses versus the partial coupling in CFSR. It is apparent that the atmosphere mostly drives the oceans outside the deep tropics (poleward of ~15°—upper two rows), and the ocean mostly drives the atmosphere in the deep tropics (especially over the equatorial Pacific—lower two rows) in the three reanalyses. It is also worth noting that the atmospheric forcing over the Atlantic and Indian Oceans penetrates deeper into the tropics than over the Pacific Ocean. The results for the two types of anomalous atmospheric forcing driving the ocean (cyclonic over cold and anticyclonic over warm anomalies) are very similar except that the frequency of cases in the mid-oceans is larger when an anticyclonic anomaly drives the ocean than when a cyclonic anomaly drives it. On the other hand the difference between the two kinds of anomalous ocean forcing driving the atmosphere shows more cases when a cold ocean forces the atmosphere than when a warm ocean does it. Also, the region where the cold ocean forces the atmosphere over the Pacific Ocean is farther to the east (even reaching the South America coasts) than the region where the warm ocean forces the atmosphere that extends more to the west of the dateline (Fig. 3, third and fourth rows from above). However the similarities in the frequency of coupled anomalies between uncoupled and coupled reanalyses suggest that the nature of the coupling between the ocean and atmosphere is transmitted via the assimilation of the observed data globally.

3.2 The ocean–atmosphere coupling under common SST anomalies and grid

Differences in the identification of the nature of the coupling from the different reanalyses may be due to several reasons, including different resolutions, differences in the analyzed observed SSTs or different sources of the observed winds and their assimilation schemes. The sources of uncertainty can be minimized by using the same observed SST anomalies for the different reanalyses at the same horizontal resolution. By using observed SST anomalies from the HadISST dataset with the vorticity anomalies from the different reanalyses on a 2.5° × 2.5° grid, any differences in the results of the use of the metrics can only be attributed to differences in the assimilation of observed winds. Figure 4 shows the frequency of coupled monthly anomalies of atmospheric and oceanic origin exceeding one local standard deviation on the common 2.5° × 2.5° grid. In this case frequencies from the two types of atmospheric and oceanic forcing are added to create a total frequency for atmospheric and oceanic forcing respectively. The general structures of the coupled anomalies are now much more similar among the different reanalyses. Frequencies of atmospheric origin (larger than 10 in count, and larger than 70 % of the total count of coupled anomalies) dominate over those of oceanic origin poleward of ~15° over the global oceans and within the tropical Indian Ocean. Frequencies of oceanic origin (larger than 10 in count, and larger than 70 % of the total count of coupled anomalies) dominate over those of atmospheric origin in the deep tropics of the Pacific Ocean and apparently in the high latitudes of the Southern Hemisphere Ocean. Some differences in the oceanic forcing within the tropics are also evident among the different reanalyses, particularly in the tropical Atlantic Ocean. This assessment of the role of the SST anomalies and horizontal resolution shows robustness to the general analysis of the coupled anomalies but points toward the differences in the assimilation of observed winds in the reanalyses as a source of uncertainty in the identification of the coupled anomalies.

3.3 The ocean–atmosphere coupling at daily and pentad scales

In addition to the analysis of the effect of the spatial resolution in the identification of the ocean–atmosphere coupling, the analysis of the impact of the temporal resolution on the regions of ocean–atmosphere coupling is also explored. Analysis of the ocean–atmosphere coupling at different temporal resolutions (monthly, pentad and daily from NOAA's OIv2 SSTs and NCEP/NCAR reanalysis vorticity) reveals the same general regions of coupling (Fig. 5). More than 70 % of the total coupled anomalies that exceed one local standard deviation arise when the atmosphere drives the ocean poleward of ~15°, as well as when the ocean drives the atmosphere in the deep tropics. The extent of the regions of coupling is reduced when the time intervals are reduced: regions exceeding 70 % of coupled anomalies are more extensive at monthly resolution than at daily resolution. The 70 % mark at pentad resolution seems to highlight the storm track regions. This analysis highlights that the atmospheric forcing is important over the Caribbean Sea and the Indian Ocean even within the 15° latitude bands. These results are corroborated

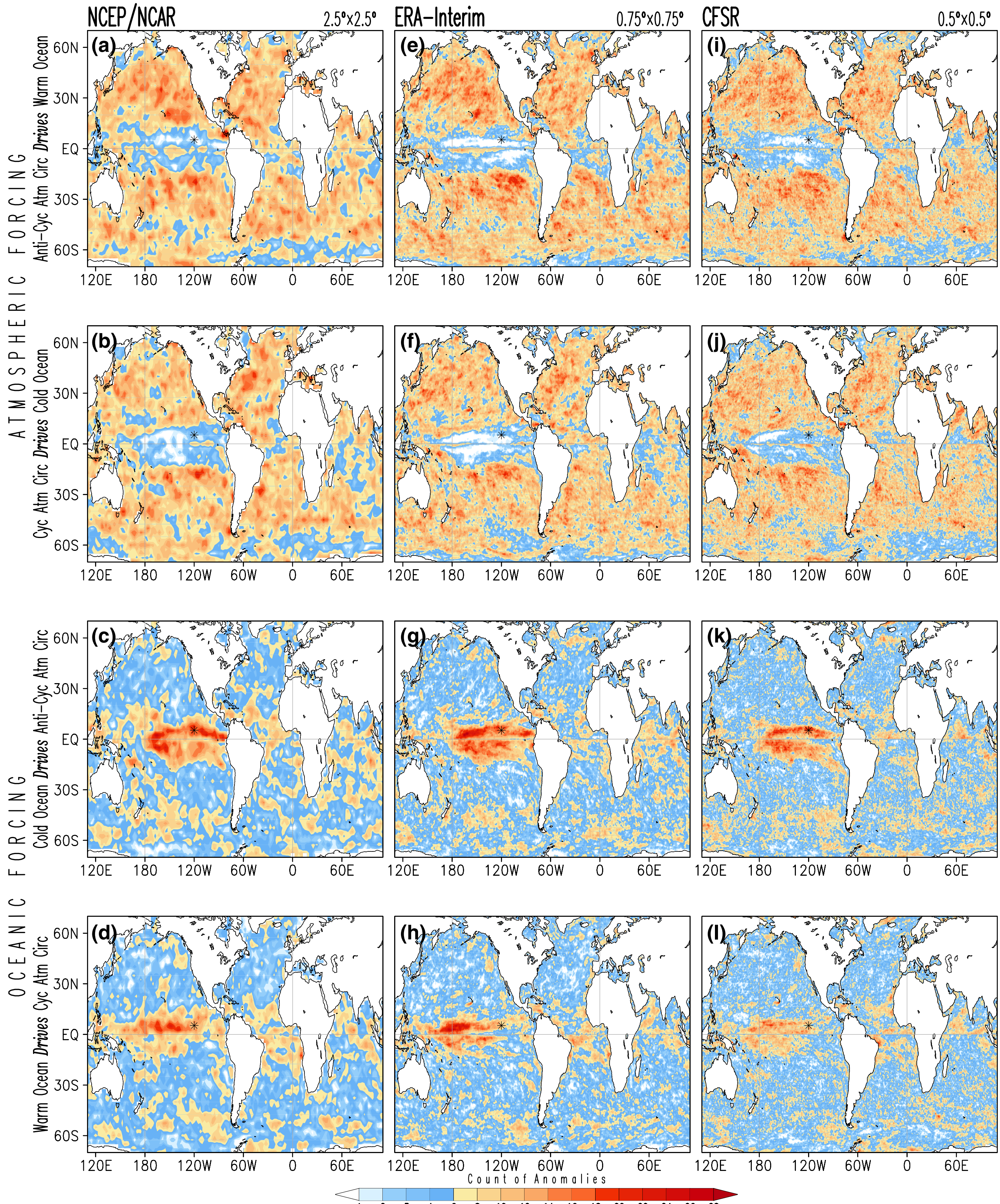
NCEP/NCAR
2.5°x2.5°
ERA-Interim
0.75°x0.75°
CFSR
0.5°x0.5°
ATMOSPHERIC FORCING
Anti-Cyc Atm Circ Drives Warm Ocean
Cyc Atm Circ Drives Cold Ocean
OCEANIC FORCING
Cold Ocean Drives Anti-Cyc Atm Circ
Warm Ocean Drives Cyc Atm Circ
(a)
(b)
(c)
(d)
(e)
(f)
(g)
(h)
(i)
(j)
(k)
(l)
60N
30N
EQ
30S
60S
120E
180
120W
60W
0
60E
Count of Anomalies
1 2 3 4 6 8 10 12 14 16 18 20 22 24 26 28

◀**Fig. 3** Frequency of coupled SST and 850 mb vorticity anomalies lasting one month in different reanalysis products for the period 1979–2004. *Left column* panels **a**–**d** are from NCAR/NCEP reanalysis, *central column* panels **e**–**h** are from ERA-Interim reanalysis, and *right column* panels **i**–**l** are from CFSR reanalysis. *Upper two rows* show the number of months when the atmosphere drives the ocean: *upper row* when an anomalous anti-cyclonic circulation in the atmosphere forces warm ocean anomalies, and *lower row* when an anomalous cyclonic circulation forces cold ocean anomalies. *Lower two rows* show the number of months when the ocean drives the atmosphere: *upper row* when an anomalous cold ocean forces an anomalous anti-cyclonic atmospheric circulation, and the *lower row* when an anomalous warm ocean forces an anomalous cyclonic atmospheric circulation. The *black asterisk* in equatorial Pacific displays the location of the grid point used for Fig. 2

when ERA-Interim's SST and vorticity data are used (not shown). Furthermore, analysis of the same daily and pentad data by BorzogMadham et al. (Manuscript in preparation) applying the Granger causality method agrees in the general distribution of the regions of atmospheric and oceanic origin of the coupled anomalies even though the physical relationship analyzed in the current analysis is not part of their method. If we assume that the reduction in the count of coupled anomalies is a direct consequence of the negative feedback mentioned earlier between atmospheric conditions (cloudy vs. sunny) and SSTs, then one could say the negative feedback gets stronger as the temporal resolution decreases from daily to monthly because the frequency of coupled anomalies lasting two time steps (2 days, 2 pentads or 2 months) is smaller with respect to the frequencies of coupled anomalies lasting one time step from monthly to daily resolution (not shown).

3.4 Contributions from ENSO, NAO, and AMO

The structure of the frequency of coupled anomalies over the equatorial Pacific from the previous analyses suggests that El Niño-Southern Oscillation (ENSO) may be an essential mode of ocean–atmosphere interactions. However, other phenomena of known atmospheric origin like the North Atlantic Oscillation (NAO) and assumed oceanic origin like the Atlantic Multidecadal Oscillation (AMO) may have less

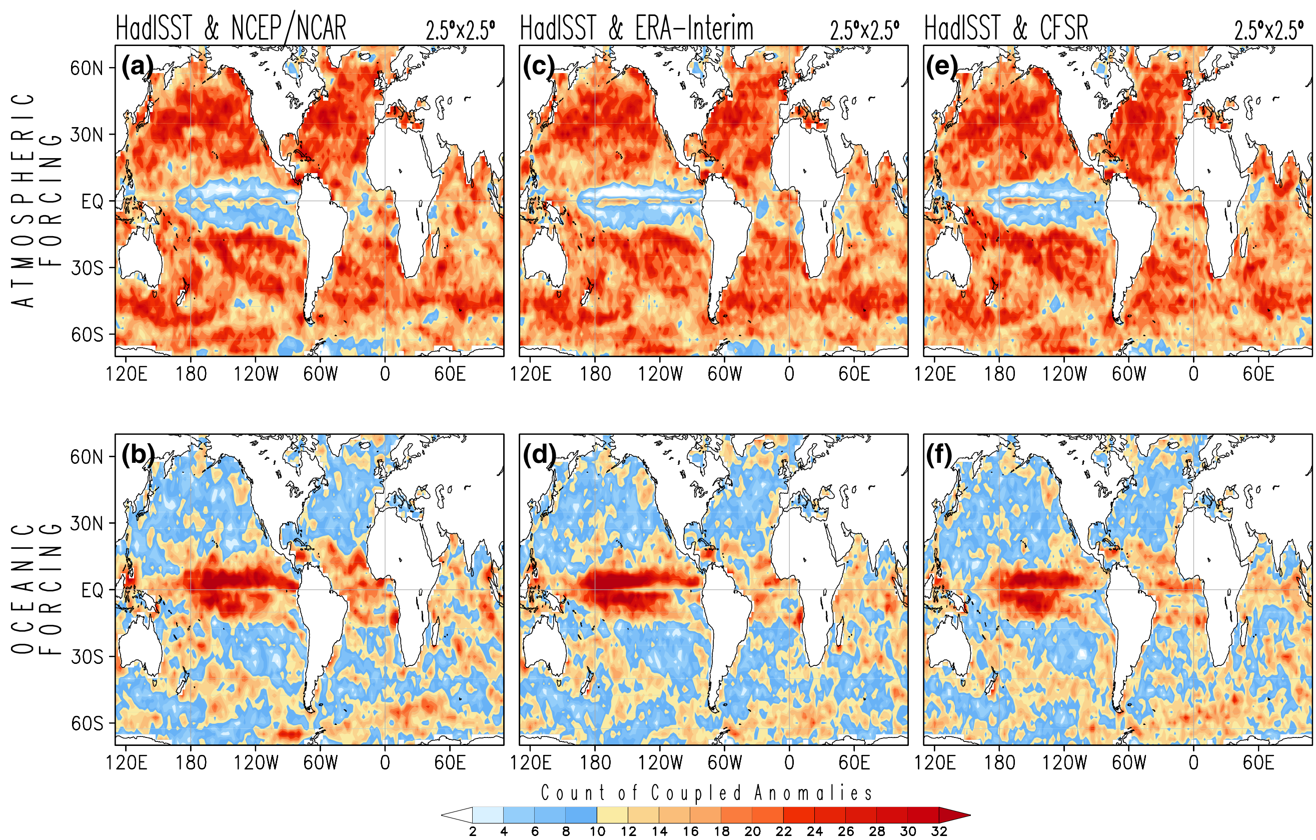

Fig. 4 Comparison of the frequency of coupled anomalies in reanalyses using the same common SST anomalies from HadISST dataset on a common 2.5° × 2.5° grid for the period 1979–2004. *Left column panels* **a**, **b** are from NCEP/NCAR, *central column* panels **c**, **d** are from ERA-Interim, and *right column* panels **e**, **f** are from CFSR reanalysis 850 mb vorticity anomalies. Simultaneous coupled anomalies are counted if they exceed the corresponding local standard deviation and last one month. The *upper row* shows the sum of the number of anomalies of the two cases when the atmosphere drives the ocean and the *lower row* shows the corresponding sum of the two cases when the ocean drives the atmosphere

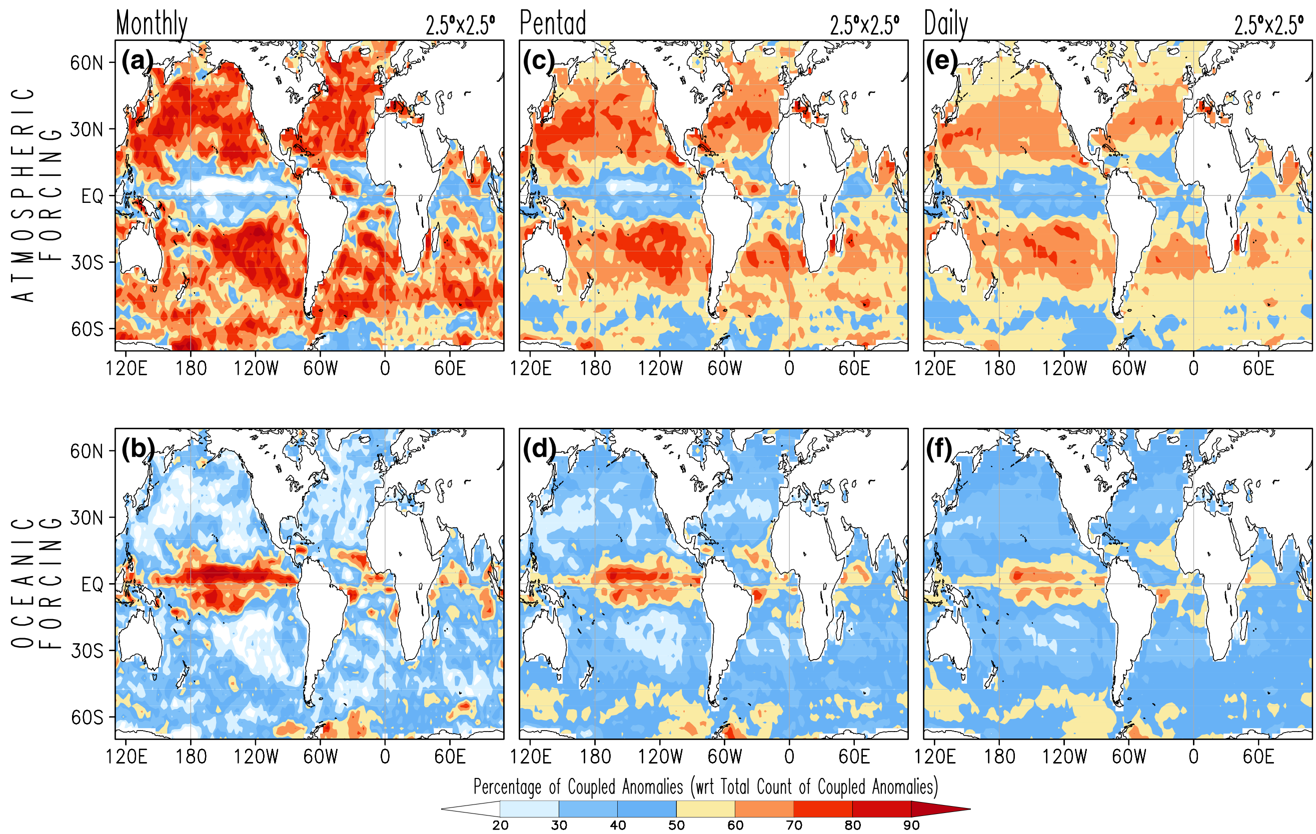

Fig. 5 Comparison of the frequency of coupled anomalies at different temporal resolutions from NOAA's OIv2 SST, and NCEP/NCAR reanalysis 850 mb vorticity anomalies for the period 1982–2013. *Left column* panels **a**, **b** are at monthly resolution, *central column* panels **c**, **d** are at pentad (5-day means) resolution, and *right column* panels **e**, **f** are at daily resolution. The number of coupled anomalies when the atmosphere drives the ocean and those when the ocean drives the atmosphere is divided by the total number of coupled anomalies (sum of times when atmosphere forces the ocean and those when the ocean drives the atmosphere) and displayed as a percentage

evident contributions to the observed frequency of coupled anomalies. In order to have a preliminary idea of the possible impact these modes of climate variability may have on the frequency of coupled anomalies, it is useful to examine the way these phenomena organize vorticity and SST anomalies (Fig. 6; see caption for additional details on the modes) before analyzing the nature of the coupled anomalies. In the case of the mature phase of ENSO (Fig. 6a, b), cyclonic anomalies along the tropical Pacific (red in the NH and blue in the SH) are associated with warm anomalies to the east of the dateline and with cold anomalies to the west. This suggests that coupled anomalies may be of oceanic origin to the east of the dateline and of atmospheric origin to the west of it. In the case of the NAO (Fig. 6c, d) the tripolar vorticity and SST anomaly structures in the Atlantic could imply coupled anomalies of atmospheric origin in the tropical and subpolar regions and of oceanic origin in the midlatitudes. Interestingly, the monopolar structure of SST anomalies and its corresponding tripolar structure in vorticity anomalies of the AMO (Fig. 6e, f) could also imply the same outcome as in the case of the NAO.

The impact of these phenomena on the frequency of coupled anomalies is investigated by first subtracting their linear regressions from the original raw SST and vorticity anomalies. Then the method is applied to on the residual SST and vorticity anomalies (Fig. 7). The total frequency of coupled anomalies with atmospheric origin exceeds the frequency of coupled anomalies with oceanic origin almost globally, except over the equatorial Pacific and some regions in the tropical Atlantic and Indian Ocean (Fig. 7, upper row). Coupled anomalies of oceanic origin make up more than 70 % of the total of coupled anomalies over the equatorial Pacific (Figs. 4, 5). By removing the influence of ENSO from the monthly anomalies the coupled anomalies of atmospheric origin are seen to increase while the coupled anomalies of oceanic origin decrease along the central equatorial Pacific, and coupled anomalies of oceanic origin increase to its east and west (Fig. 7c, d). The strong signal of ENSO along the equatorial Pacific is partially due to the oceanic nature of the NINO3.4 index used to characterize it. If the Southern Oscillation Index (a sea level pressure based index) is used instead of the NINO3.4 index,

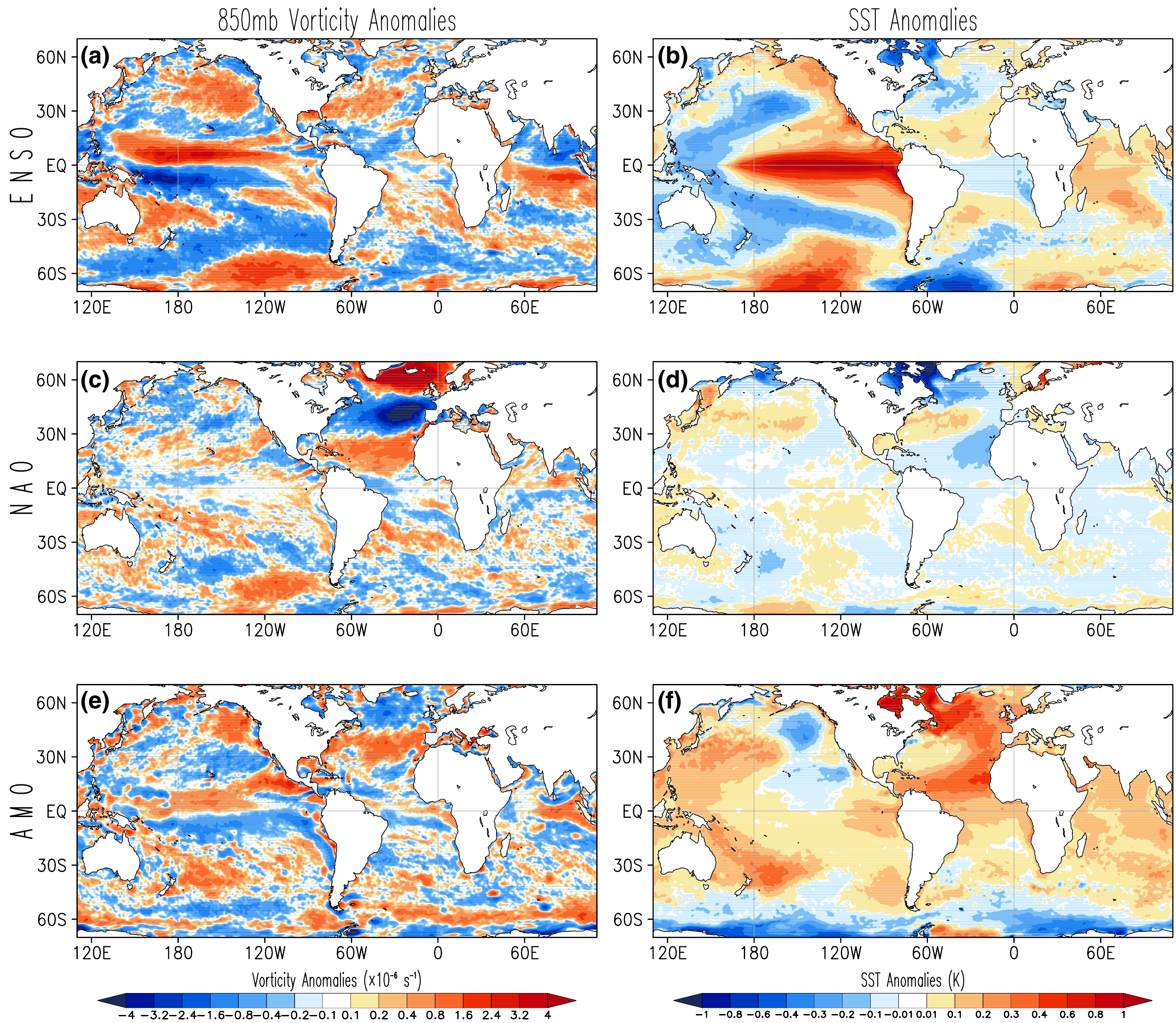

Fig. 6 Linearly regressed vorticity at 850 mb and SST anomalies associated to ENSO, NAO and AMO for the period 1979–2004 from CFSR reanalysis. Anomalies from ENSO are in the *upper panels* for **a** vorticity, and **b** SST; anomalies from the NAO are in the *middle panels* for **c** vorticity, and **d** SST; anomalies from the AMO are in the *bottom panel* for **e**) vorticity, and **f** SST. ENSO is characterized by the NINO3.4 index calculated as area-averaged SST anomalies over the region [170°–120°W, 5°S–5°N] from the HadISST data set. The NAO is characterized by Hurrell's sea level pressure station-based NAO index (Hurrell 1995). The AMO is characterized by the AMO index calculated as area-averaged linearly detrended SST anomalies over the region [75°–5°W, 0°–60°N] from the HadISST data set. The simultaneous regressions represent the mature phase of each phenomenon. Units are s^{-1} for vorticity and K for SST anomalies

the signal is somewhat reduced. This results in less coupled anomalies of atmospheric origin, and more of oceanic origin, in the south equatorial region (180°–110°W; not shown) than seen when using the NINO3.4 index. These results suggest that in the absence of ENSO, or an erroneous forecast of it, the potential for teleconnections and thus the predictability that arises from equatorial Pacific SST anomalies will be largely reduced as the coupled anomalies of oceanic origin are reduced in favor of the anomalies of atmospheric origin.

The impact of the NAO and AMO in the frequency of coupled anomalies extends from the tropics to the midlatitudes of the Atlantic Ocean (Fig. 7, lower two rows) although its impact is weaker over the equatorial Pacific than the impact from ENSO. The absence of these two phenomena mimic their surface signatures with a tripolar structure of alternating signs confined to the midlatitudes for the NAO (Fig. 7e, f) and the whole North Atlantic for the AMO (Fig. 7g, h). Specifically, the absence of the NAO increases coupled anomalies of atmospheric origin around

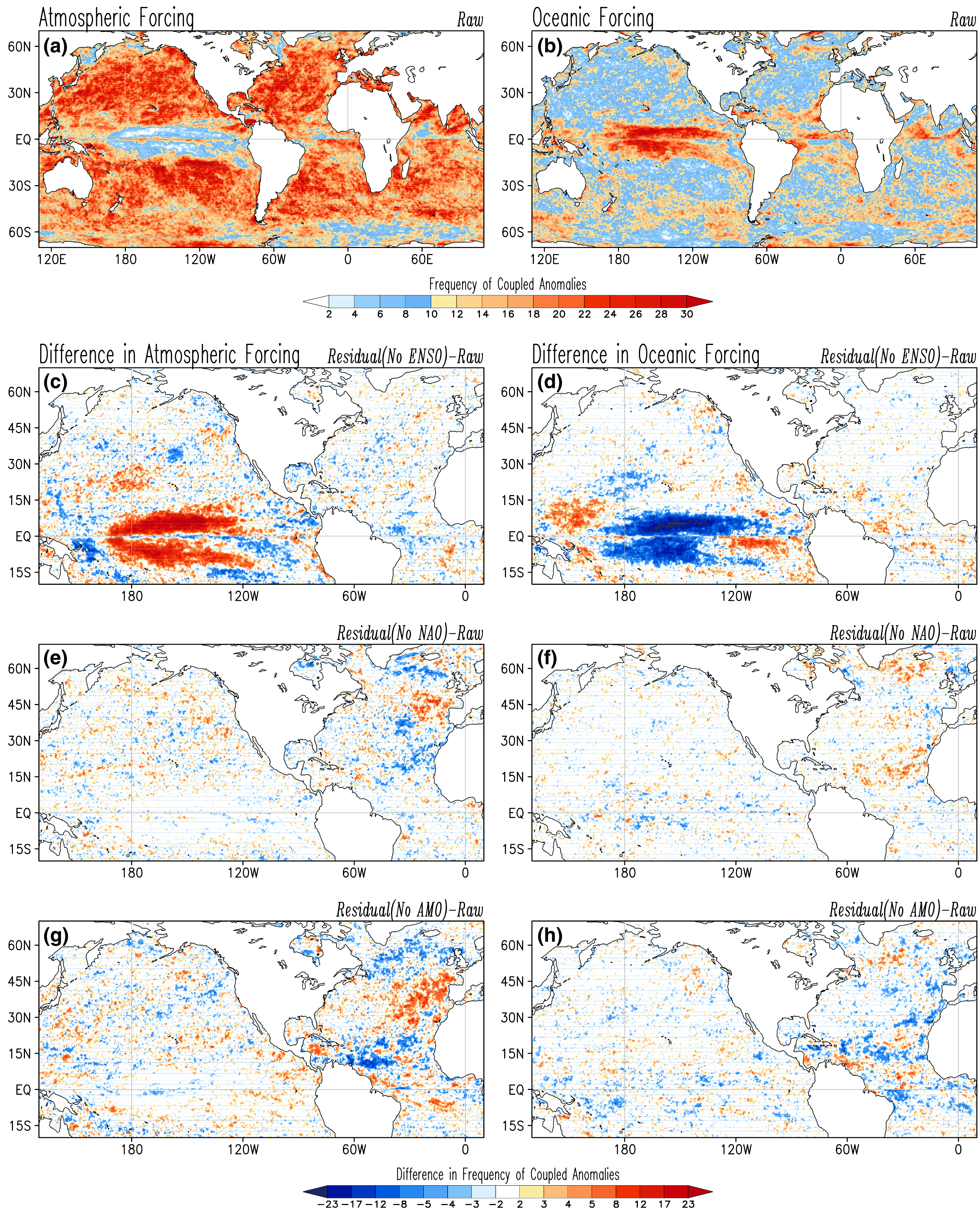

Atmospheric Forcing
Raw
Oceanic Forcing
Raw
(a)
(b)
60N
30N
EQ
30S
60S
120E
180
120W
60W
0
60E
Frequency of Coupled Anomalies
2 4 6 8 10 12 14 16 18 20 22 24 26 28 30
Difference in Atmospheric Forcing
Residual(No ENSO)-Raw
Difference in Oceanic Forcing
Residual(No ENSO)-Raw
(c)
(d)
45N
15N
15S
Residual(No NAO)-Raw
(e)
(f)
Residual(No AMO)-Raw
(g)
(h)
Difference in Frequency of Coupled Anomalies
−23 −17 −12 −8 −5 −4 −3 −2 2 3 4 5 8 12 17 23

◀**Fig. 7** Comparison of the frequency of coupled SST and 850 mb vorticity anomalies lasting at least one month when ENSO, NAO, and AMO are excluded from the CFSR reanalysis dataset for the period 1979–2004. *Upper row* displays the total frequency of coupled *raw* anomalies lasting one month when **a** the atmosphere drives the ocean, and **b** the ocean drives the atmosphere; these frequencies are subtracted from the frequencies of coupled *residua*l anomalies. *Second row* from the *top* shows the difference in frequencies obtained from the coupled *No-ENSO residua*l anomalies and those from the original raw anomalies when **c** the atmosphere drives the ocean, and **d** when the ocean drives the atmosphere. *Third row* from the *top* shows the difference in frequencies obtained from coupled *No-NAO residua*l anomalies and those from the original raw anomalies when **e** the atmosphere drives the ocean, and **f** when the ocean drives the atmosphere. *Fourth row* from the *top* shows the difference in frequencies obtained from coupled *No-AMO residua*l anomalies and those from the original raw anomalies when **g** the atmosphere drives the ocean, and **h** when the ocean drives the atmosphere. Residual anomalies are obtained by subtracting the linearly regressed anomalies of the indices from the original raw SST and vorticity anomalies. *Blue/red shading* in the panels of differences identifies regions where the absence of the phenomenon produces less/more coupled anomalies than the raw reference case

45°N close to Europe, and decreases coupled anomalies to the north and south of it. The absence of the AMO also produces increased coupled anomalies of atmospheric origin between 30°N and 45°N closer to Europe, and decreased coupled anomalies to the north and south but reaching the tropical Atlantic in this case. It is worth noting that correlations of the NAO and AMO with global 850 mb vorticity and SST anomalies have contrasting magnitudes in the Atlantic (not shown): while the NAO has a stronger correlation with vorticity than with SST anomalies, the AMO presents the opposite relationship; this can only be due to the intrinsic atmospheric nature of the NAO, and the oceanic nature of the AMO. Despite differences in the Atlantic, in both cases, anomalies span tropical latitudes, midlatitudes and subpolar latitudes. Thus omission of the NAO and AMO would result in a decrease of coupled anomalies of atmospheric origin in the polar and tropical latitudes and an increase in the midlatitudes, as well as an increase in the coupled anomalies of oceanic origin in the polar and tropical latitudes and a decrease in the midlatitudes even though the signal is somewhat noisy.

4 Ocean–atmosphere coupling in model simulations and decadal predictions

The previous section established the nature of the ocean–atmosphere coupling as seen by the different reanalyses products. The agreement among the reanalyses, despite their differences, suggests that the regions of coupling identified as being of atmospheric or oceanic origin are robust, and the method provides the basis to assess the ocean–atmosphere coupling in climate models. The fact that there are no major differences among the reanalyses in the global frequency of the coupled anomalies indicates that the nature of the coupling in the different atmospheric reanalyses (two are uncoupled and one is weakly coupled) can be transmitted via the assimilation of observed data. This suggests a major difference will be observed in the AMIP style simulations, because the atmosphere is influenced by the ocean but cannot force back the ocean with any feedback and most importantly there is not update of simulated atmospheric fields with observations as in reanalyses.

4.1 Comparisons between coupled and atmospheric (AMIP) simulations

The use of the metric on the coupled ocean–atmosphere simulations should provide information on the the way the models incorporate the characterized local dynamical ocean–atmosphere coupling. Application of the metric on AMIP-style simulations should also allow assessing the role of the absent atmospheric forcing.

Knowing that the CMIP5 models used no flux adjustments, assessment of the coupling in the annual cycle of SST and vorticity will provide an accurate estimation of biases in the coupling. The coupling in historical and AMIP simulations of the twentieth century climate from the CMIP5 models is compared to the coupling identified using HadISST's SSTs and CFSR's vorticities to minimize biases due the analyzed SSTs in the reanalysis. To review, the CMIP5 historical simulations are simulations done with coupled ocean–atmosphere models so the two-way interactions are present in these types of simulations. On the other hand, the AMIP-style simulations are carried out with the atmospheric model used in the coupled simulations and forced with observed SSTs creating a one-way interaction from the ocean to the atmosphere and preventing the feedback interaction from the atmosphere to the ocean (Table 1).

Exploration of the coupled anomalies forced by the atmosphere (Fig. 8) shows that the coupled simulations of the twentieth century climate (Fig. 8, top and left panels) depict the broad features seen in the metric from observations. Some marked differences appear over the minimum around the equatorial Pacific as well as the coverage of the high count of coupled anomalies over the Pacific and Atlantic oceans on both hemispheres. This discrepancy is most prominent over the South Pacific and Atlantic Convergence Zones (SPCZ & SACZ) and the Maritime Continent. For instance, the region over the SPCZ has a high count of coupled anomalies in observations, but this is not the case in the coupled simulations to the west of ~120°W where the count is much smaller in the four models. On the other hand, an unrealistic storm track in the Southern Hemisphere seems to be a very well defined feature in three of the four models as

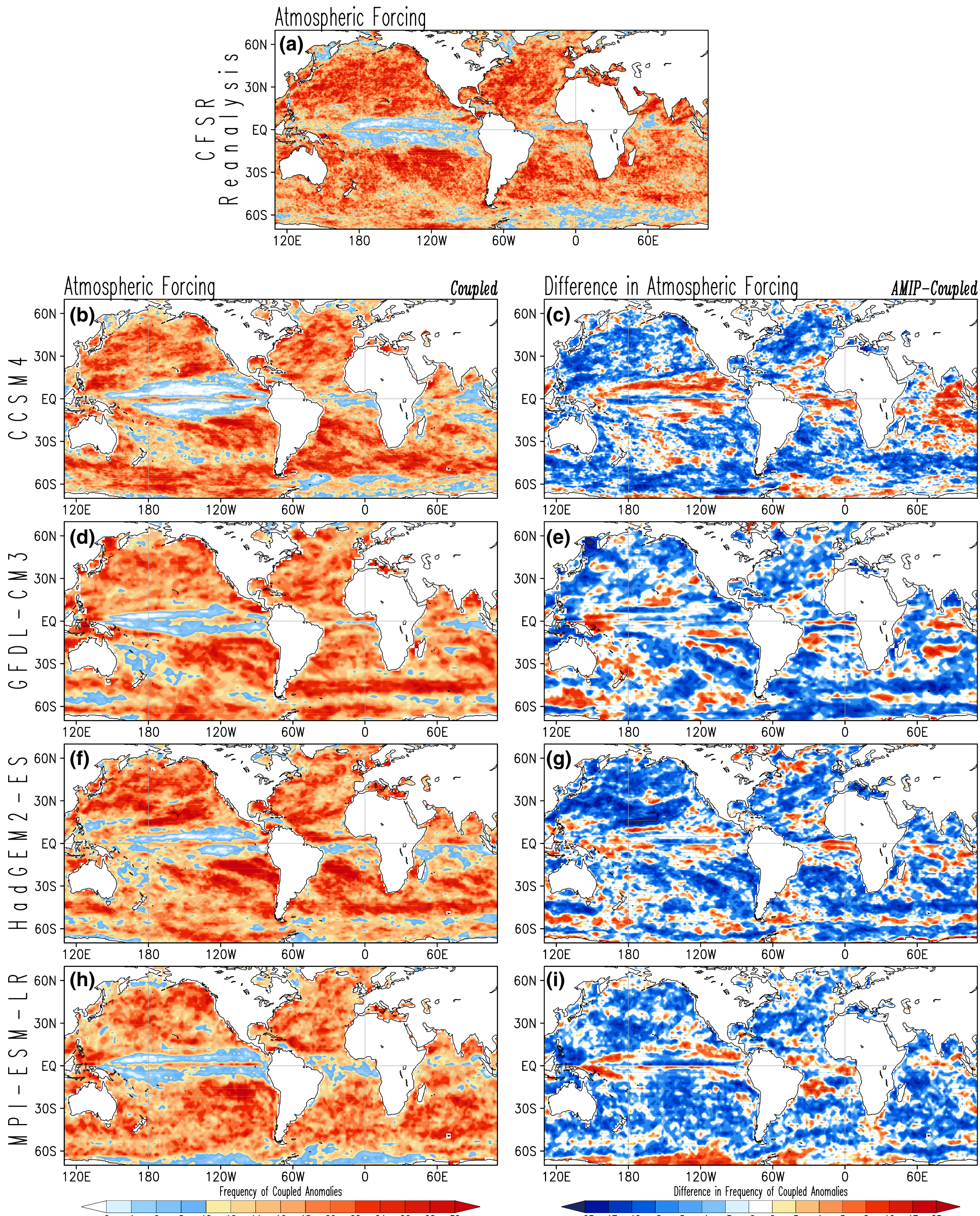
Atmospheric Forcing
CFSR Reanalysis
(a)
60N
30N
EQ
30S
60S
120E
180
120W
60W
0
60E
Atmospheric Forcing
Coupled
Difference in Atmospheric Forcing
AMIP-Coupled
CCSM4
(b)
(c)
GFDL-CM3
(d)
(e)
HadGEM2-ES
(f)
(g)
MPI-ESM-LR
(h)
(i)
Frequency of Coupled Anomalies
2 4 6 8 10 12 14 16 18 20 22 24 26 28 30
Difference in Frequency of Coupled Anomalies
−23 −17 −12 −8 −5 −4 −3 −2 2 3 4 5 8 12 17 23

◀**Fig. 8** Comparison of the frequency of the coupled SST and 850 mb vorticity anomalies lasting one month when the atmosphere drives the ocean in CFSR reanalysis and *Coupled (historical)* and *AMIP* (uncoupled) simulations of the twentieth century climate from CMIP5 models for the period 1979–2004. Total frequency of coupled anomalies are displayed in **a** from HadISST's SSTs and CFSR's vorticities, and *left column* panels from historical coupled model simulations by **b** CCSM4, **d** GFDL-CM3, **f** HadGEM2-ES and **h** MPI-ESM-LR models. The frequencies from the coupled simulations are subtracted from the frequencies from the ocean-forced AMIP atmospheric simulations and are displayed in the *right column* panels from **c** CCSM4, **e** GFDL-CM3, **g** HadGEM2-ES and **i** MPI-ESM-LR models. *Blue/red shading* in the panels of differences identifies regions where the lack of the atmosphere feedback to the ocean in the AMIP simulations produces less/more coupled anomalies than the coupled simulations reference case

portrayed by the region of high count of coupled anomalies around 50°S. This feature is not seen in observations.

When the interaction from the atmosphere to the ocean is turned off in the AMIP simulations (Fig. 8, right column panels), as could be expected, a large decrease in the number of coupled anomalies forced by the atmosphere is apparent when compared with the frequency of coupled anomalies from the coupled simulations. However, there is also a spurious increase in the coupled anomalies of atmospheric origin within the tropics. The spurious increase in coupled anomalies of atmospheric origin in the AMIP simulations occurs in these regions where the frequency of coupled anomalies are at a minimum in the coupled simulation (compare left vs. right panels in Fig. 8). The increase of coupled anomalies of atmospheric origin in the AMIP simulations is counterintuitive as the ocean model has no means to respond to the atmosphere locally. Thus the appearance of these anomalies is artificial and likely due to the nonlocal generation of the vorticity anomalies.

In general, regions in the tropics with a high count of coupled anomalies of oceanic origin typically have a low count of coupled anomalies of atmospheric origin (Figs. 9 vs. 8, upper panels). This is in agreement with the notion that anomalies driven by the ocean are longer lasting. These are found in the deep tropics, with the equatorial Pacific having the largest counts, followed by the tropical Atlantic and then the equatorial Indian Ocean. There are fewer observed coupled anomalies over the SPCZ and south Atlantic storm track. Assessment of the coupled anomalies of oceanic origin from the coupled simulations (Fig. 9, left panels) shows clearly emphasized the equatorial regions as well the southern midlatitudes. Notable differences, like the anomalous high count over the equatorial and southern Indian Ocean in CCSM4 or over the SPCZ in the CCSM4 and GFDL-CM3, or over the southern tropical Atlantic are also apparent. The anomalous high count of anomalies of atmospheric origin identified over the southern storm track region is also identified in this case of coupled anomalies of oceanic origin but displaced ~10° farther to the south (CCSM4, GFDL-CM3 and HadGEM2-ES). Artificial coupling driven by the ocean is generated in the midlatitudes when the feedback from the atmosphere to the ocean is turned off in the AMIP simulations (Fig. 9, right panels). Artificial coupling forced from the ocean to the atmosphere is generated almost everywhere but notably in the midlatitudes when the feedback from the atmosphere to the ocean is shut down in the AMIP simulations (Fig. 9 right panels).

In general it is remarkable the consistence between the results from the coupled simulations and reanalyses in spite of the differences in SSTs, their treatment, and the models. These findings are in line with those by Meehl et al. (2004) indicating that the atmospheric model can manage the important global feedbacks (and coupling) between the atmosphere and ocean only in a coupled model. In addition, the large differences in the ocean–atmosphere coupling between the fully coupled, or reanalyses, and AMIP simulations confirms the idea that the nature of the coupling in the uncoupled reanalyses is transmitted via the assimilation of observed atmospheric fields.

4.2 Decadal prediction

In 30-year hindcast experiments, since they use coupled models, one would expect to find an active ocean–atmosphere coupling despite the presence of the greenhouse gases. However, analysis of the decadal prediction available from CCSM4 gives unexpected results (Fig. 10). It is found that the coupled anomalies of atmospheric origin are notably reduced outside of the deep tropics and artificially increased in the deep tropics (Fig. 10e). Conversely, the coupled anomalies of oceanic origin are artificially increased outside of the tropics and notably reduced in the tropics (Fig. 10f). It has already been established that the AMIP simulations have reduced coupled anomalies of atmospheric origin over large areas of the global oceans. AMIP simulations also spuriously augment the number of coupled anomalies of atmospheric origin in the tropics and the coupled anomalies of oceanic origin over large areas of the global oceans even at midlatitudes (such anomalies are not present in observations or coupled simulations). Analysis of the 30-year hindcast indicates frequencies of coupled anomalies that resemble those from the AMIP simulation but with a much weaker oceanic forcing in the deep tropics. Division of the hindcast in three smaller periods of 8 years each (not shown) indicates not only that the initial surface conditions have no impact in the frequency of coupled anomalies especially in the first of the periods, but also that the hindcast is unable to have a realistic count of coupled anomalies as the coupled simulation through the other 8-year periods. These results indicate that this coupled hindcast is not realistic, since it should reproduce the atmospheric–ocean coupling basically as in the CMIP5 coupled (historical) runs or in the reanalyses.

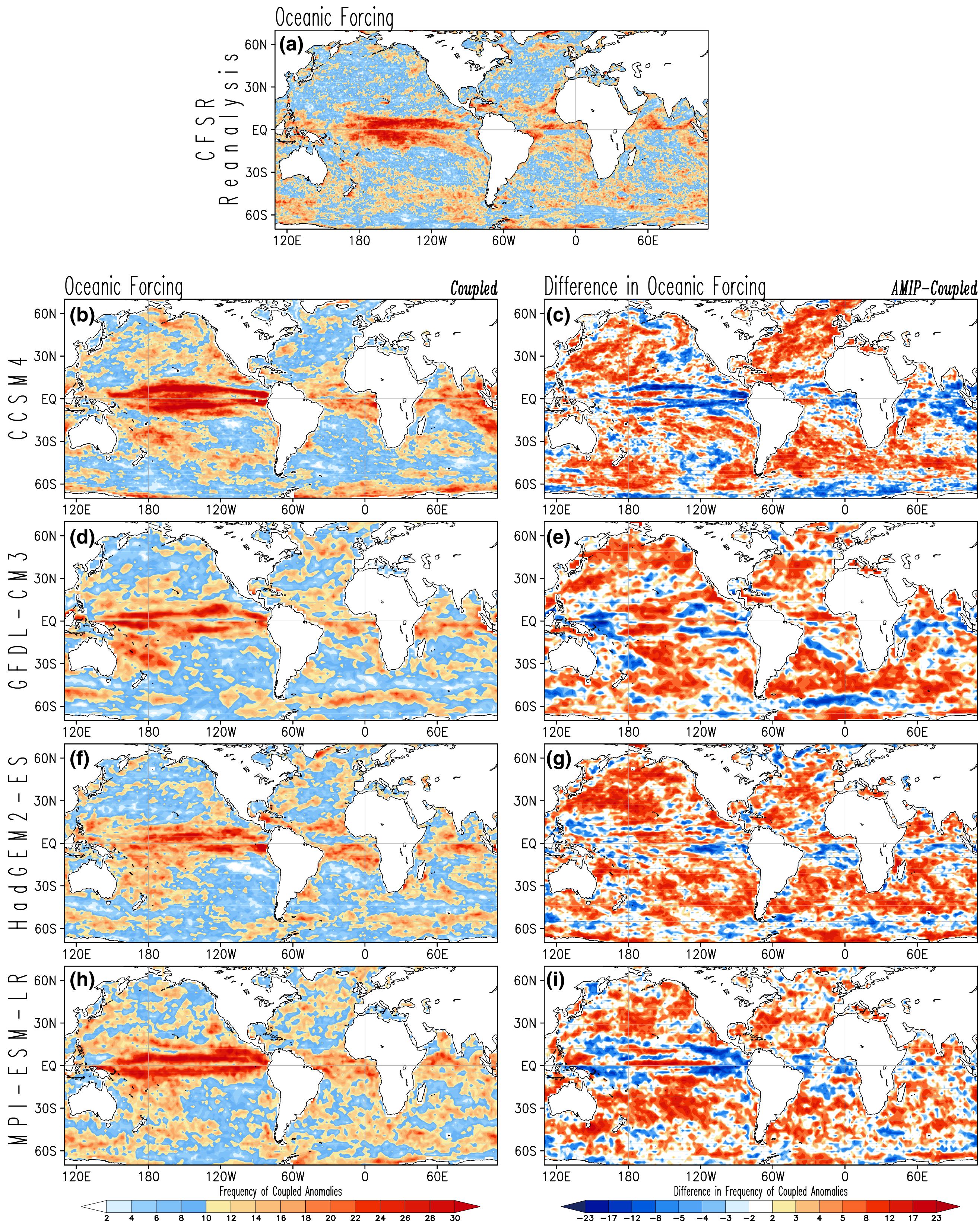
Oceanic Forcing
CFSR Reanalysis
(a)
Oceanic Forcing
Coupled
Difference in Oceanic Forcing
AMIP-Coupled
CCSM4
(b)
(c)
GFDL-CM3
(d)
(e)
HadGEM2-ES
(f)
(g)
MPI-ESM-LR
(h)
(i)
60N
30N
EQ
30S
60S
120E
180
120W
60W
0
60E
Frequency of Coupled Anomalies
2 4 6 8 10 12 14 16 18 20 22 24 26 28 30
Difference in Frequency of Coupled Anomalies
−23 −17 −12 −8 −5 −4 −3 −2 2 3 4 5 8 12 17 23

◀**Fig. 9** Comparison of the frequency of coupled SST and 850 mb vorticity anomalies lasting one month when the ocean drives the atmosphere in CFSR reanalysis and *Coupled* (*historical)* and *AMIP* simulations of the twentieth century climate from CMIP5 models for the period 1979–2004. Total frequency of coupled anomalies are displayed in **a** from HadISST's SSTs and CFSR's vorticities, and *left column* panels from historical coupled model simulations from **b** CCSM4, **d** GFDL-CM3, **f** HadGEM2-ES and **h** MPI-ESM-LR models. The frequencies from the coupled simulations are subtracted from the frequencies from the ocean-forced AMIP atmospheric simulations and are displayed in the *right column* panels from **c** CCSM4, **e** GFDL-CM3, **g** HadGEM2-ES and **i** MPI-ESM-LR models. *Blue/red shading* in the *right column* panels of differences identifies regions where the lack of the atmosphere feedback to the ocean in the AMIP simulations produces less/more coupled anomalies than the coupled simulations reference case

5 Summary and concluding remarks

The present analysis first investigates the robustness of the physical method devised by Kalnay et al. (1986) and later used by Peña et al. (2003) to identify locally the driver in coupled ocean–atmosphere anomalies. The method identifies coupled anomalies as of atmospheric origin if cyclonic anomalies in vorticity at 850 mb are located over cold SST anomalies, or anticyclonic anomalies are over warm SST anomalies. Conversely, anomalies of oceanic origin are identified if cyclonic anomalies are located over warm SST anomalies or anticyclonic anomalies are over cold SST anomalies. The method does not attempt to be inclusive of all types of coupling in nature and it benefits of the local relationship between the atmospheric and oceanic variables with no consideration of the large scale coupling as in the case of the atmospheric circulation forcing SST anomalies along the coasts. Second, the method is applied as a metric to assess the coupling in climate simulations and predictions from models participating in the CMIP5 project.

Comparisons of uncoupled (NCEP/NCAR and ERA-Interim) and partially coupled (CFSR) reanalyses, indicates that the results are robust. The frequency of coupled anomalies of atmospheric origin is larger than those of oceanic origin on large portions of the global oceans, except over the deep tropics in the Pacific, and some portions of the Atlantic and Indian Oceans. This result was agreed upon between the different reanalyses products. Partitioning of the frequency of coupled anomalies of atmospheric origin shows that those from anticyclones driving warm sea surface anomalies produce slightly more cases than those from cyclones driving cold sea surface anomalies. On the other hand, partitioning of the frequency of coupled anomalies of oceanic origin shows that those from cold sea surface anomalies driving anticyclonic circulation anomalies in the tropics produce more cases than those from warm surface anomalies driving cyclonic circulation anomalies. The latter has a focus farther to the west in the equatorial Pacific closer to the Warm Pool. Similarities in the frequencies of coupled anomalies between the uncoupled reanalyses and the partially coupled reanalysis indicate that the nature of the coupling is transmitted to the atmosphere by the assimilation of observed data (e.g., winds). When a common observed SST dataset is paired with the vorticities of the different reanalyses on a common grid, the differences between the reanalyses becomes much smaller and attributable to differences in the amount and mode that the observed data is assimilated in the atmospheric reanalyses.

The regions of coupling when the atmosphere drives the ocean and vice versa occupy similar regions in the global oceans independent of their temporal resolutions. Nevertheless, the anomalies are more frequent and extensive at monthly resolution than at pentad (5-day means) or daily resolutions. This difference is presumably due to the larger variability present at the higher temporal resolutions. Analysis of the same daily and pentad data applying the Granger causality method, which does not need of the physical phase relationship between SST and vorticity anomalies, agrees well within the general distribution of the regions of atmospheric and oceanic origin of the coupled anomalies.

Exclusion of known phenomena like ENSO, NAO and AMO has some regional effects on the distribution of coupled anomalies. The absence of ENSO, which has the strongest effect, increases the frequency of coupled anomalies of atmospheric origin and decreases that of oceanic origin in the central tropical Pacific. This region coincides with the region where the characteristic anomalies of ENSO are maximum for vorticity rather than for SST (located farther to the east). The reduction of coupled anomalies of oceanic origin in the absence of ENSO is not surprising since it is known that ENSO creates equatorial Pacific SST anomalies that are an important forcing of atmospheric teleconnections. In this light, it is clear that the absence of ENSO, or an erroneous simulation/forecast of it, will reduce atmospheric teleconnections, global climate variability as well as climate predictability. The absence of the NAO has a much smaller impact on the frequencies of coupled anomalies compared to the absence of ENSO. The region of impact of the absence of the NAO follows the regions of the regressed vorticity anomalies over the midlatitudes of the North Atlantic: an increase of coupled anomalies of atmospheric origin in front of the European coasts around 45°N, and a decrease of them to its north and south; the opposite effect is seen in the frequency of coupled anomalies of oceanic origin. The absence of the AMO on the other hand has a more extensive effect on the frequency of coupled anomalies than the absence of the NAO but still much less than the absence of ENSO. In this case, the frequency of coupled anomalies of atmospheric origin follows the regions of regressed SST anomalies with an

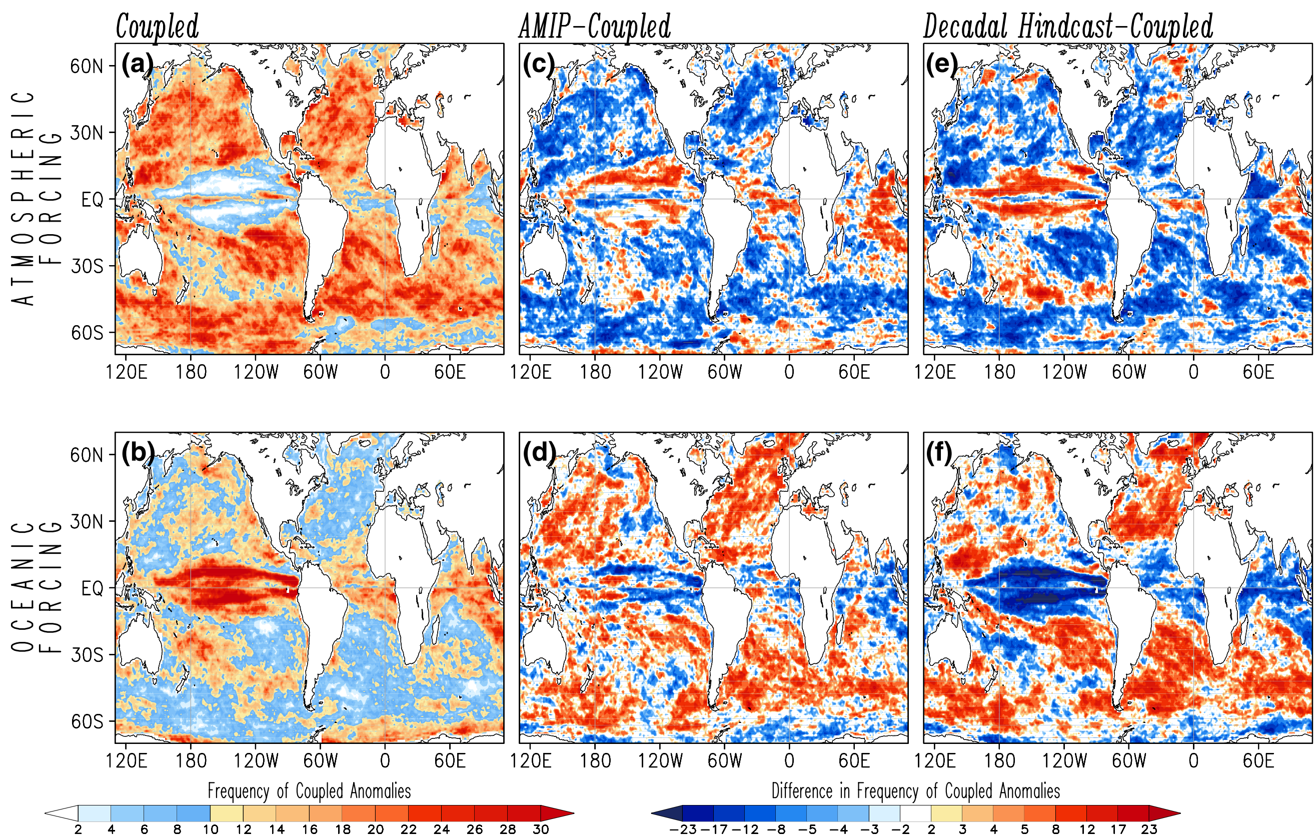

Fig. 10 Comparison of the frequency of coupled SST and 850 mb vorticity anomalies lasting one month in CMIP5's CCSM4 *Coupled* (*historical*) and *AMIP* simulations of the twentieth century climate and 30-year *Coupled Decadal Hindcast* for the period 1980–2004. Total frequency of coupled anomalies when the atmosphere drives the ocean is in the *upper row* and when the ocean drives the atmosphere in the *lower row*. Frequencies for the coupled simulation are in panels **a**, **b**, differences in frequencies from AMIP simulation with respect to the frequencies from the coupled simulations are in panels **c**, **d**, and differences in frequencies from the 30-year coupled decadal hindcast initialized in 1980 with respect to the frequencies from the coupled simulations are in panels **e**, **f**. *Blue/red shading* in the panels of differences identifies regions where the AMIP simulation and decadal hindcast produce less/more coupled anomalies than the historical coupled simulations reference case

increase in anomalies of atmospheric origin in the subtropics near the African and European costs, and a decrease in the frequency to the north and south of this region up to the Caribbean region. The frequency of anomalies of oceanic origin experiences the opposite gain and decrease over the regions mentioned for the anomalies of atmospheric origin. For both NAO and AMO, the frequency of the coupled anomalies of oceanic origin is less than those from atmospheric origin if these modes of climate variability are excluded.

Analysis of the frequency of coupled anomalies from the CMIP5 simulations gives a coherent picture. Analysis of the coupled (historical) simulations of the twentieth century climate indicates the climate models in general agree with the distribution of anomalies of atmospheric and oceanic origin as mentioned above although regional differences are evident. On the other hand, the lack of the feedback from the atmosphere to the ocean in the AMIP simulations decreases the appearance of coupled anomalies of atmospheric origin but artificially increase those in the tropics presumably due to the nonlocal (i.e., remote) generation of vorticity anomalies. In turn, the frequency of the anomalies of oceanic origin are decreased in the tropics and artificially increased outside the tropics. Differences in the frequency of coupled anomalies between the AMIP-style simulations and those from the uncoupled reanalyses support the idea that the nature of the coupling between the ocean and the atmosphere identified in the reanalyses is transmitted via the assimilation of the observed data which is absent in the AMIP simulations.

However, analysis of the only available 30-year hindcast with a coupled model from the CMIP5 project reveals unexpected results as they are closer to an AMIP simulation than to a coupled simulation even though it is documented as using a coupled model. The frequency of coupled anomalies from the 30-year hindcast resembles that from AMIP simulation but it is further deteriorated in the deep tropics where the oceanic forcing is much weaker than in the historical or AMIP simulations. This resemblance in the coupled anomalies between the hindcast and AMIP simulations is surprising as it was expected to find more similarities in the coupled anomalies identified with the coupled (historical) simulation and reanalyses. Therefore, the climate hindcast or prediction seems to be unrealistic as it has reduced presence of coupled anomalies of atmospheric origin globally and a large reduction of coupled anomalies of oceanic origin in the tropics. The latter suggests the existence of artificially generated anomalies of atmospheric origin that minimize the role that the tropics may play in the prediction. The diagnosis of the hindcast behaving more like an AMIP simulation than a coupled simulation has been only possible with the use of this metric that indentifies the origin of coupled anomalies. This issue with the hindcast will be explored further by applying the metric to an extended group of hindcasts.

Acknowledgments We gratefully acknowledge support from NSF grant CMMI1125285, NASA grants NNX11AL25G, NNX13AG68G and NOAA grant CICS-PAEK-LETKF11. AR-B also wishes acknowledge support from NSF grant AGS1439940. SM received support from the National Socio-Environmental Synthesis Center (SESYNC)—NSF award DBI-1052875. SM also acknowledges support from the University of Maryland Council on the Environment. We thank Laura Bracaglia for her helpful suggestions that improved the text of the paper. We also thank two anonymous reviewers for the valuable comments that helped to improve the manuscript. We would like to acknowledge the World Climate Research Programme's Working Group on Coupled Modeling, which is responsible for CMIP. We acknowledge the climate modeling groups (listed in the Data section) for producing and making available their model outputs. For CMIP the U.S. Department of Energy's Program for Climate Model Diagnosis and Intercomparison provides coordinating support and leads development of the necessary software infrastructure in partnership with the Global Organization for Earth System Science Portals. We acknowledge the modeling groups, the Program for Climate Model Diagnosis and Intercomparison (PCMDI) and the WCRP's Working Group on Coupled Modeling (WGCM) for their roles in making available the WCRP CMIP5 multi-model dataset. Support for this dataset is provided by the Office of Science, U.S. Department of Energy.

References

Barsugli JJ, Battisti DS (1998) The basic effects of atmosphere-ocean thermal coupling on midlatitude variability. J Atmos Sci 55:477–493

Bellenger H, Guilyardi E, Leloup J, Lengaigne M, Vialard J (2014) ENSO representation in climate models: from CMIP3 to CMIP5. Clim Dyn 42:1999–2018. doi:10.1007/s00382-013-1783-z

Bjerknes J (1969) Atmospheric teleconnections from the equatorial Pacific. Mon Wea Rev 97:163–172

Bryan K, Stouffer R (1991) A note on Bjerknes' hypothesis for North Atlantic variability. J Marine Syst 1:229–241

Collins WJ et al (2008) Evaluation of the HadGEM2 model. Met Office Hadley Centre Technical Note no. HCTN 74, available from Met Office, FitzRoy Road, Exeter EX1 3 PB. http://www.metoffice.gov.uk/publications/HCTN/index.html

Davini P, Cagnazzo C (2013) On the misinterpretation of the North Atlantic Oscillation in CMIP5 models. Clim Dyn 43:1497–1511. doi:10.1007/s00382-013-1970-y

Dee DP et al (2011) The ERA-Interim reanalysis: configuration and performance of the data assimilation system. Quart J R Meteorol Soc 137:553–597. doi:10.1002/qj.828

Deser C, Alexander MA, Xie S-P, Phillips A (2010) Sea surface temperature variability: patterns and mechanisms. Annu Rev Marine Sci 2:115–143

Donner LJ et al (2011) The dynamical core, physical parameterizations, and basic simulation characteristics of the atmospheric component of the GFDL global coupled model CM3. J Clim 24:3484–3519. doi:10.1175/2011JCLI3955.1

Gates WL (1992) AMIP: the atmospheric model intercomparison project. Bull Am Meteor Soc 73:1962–1970

Gent PR et al (2011) The Community Climate System Model Version 4. J Clim 24:4973–4991. doi:10.1175/2011JCLI4083.1

Griffies SM et al (2011) The GFDL CM3 coupled climate model: characteristics of the ocean and sea ice simulations. J Clim 24:3520–3544. doi:10.1175/2011JCLI3964.1

Hurrell JW (1995) Decadal trends in the North Atlantic Oscillation: regional temperatures and precipitation. Science 269:676–679

IPCC (2013) Climate change 2013: the physical science basis. In: Stocker TF, Qin D, Plattner G-K, Tignor M, Allen SK, Boschung J, Nauels A, Xia Y, Bex V, Midgley PM (eds) Contribution of working group I to the fifth assessment report of the intergovernmental panel on climate change. Cambridge University Press, Cambridge

Kalnay E, Mo KC, Paegle J (1986) Large-amplitude, short-scale stationary Rossby waves in the Southern Hemisphere: observations and mechanistic experiments to determine their origin. J Atmos Sci 43:252–275

Kalnay E et al (1996) The NCEP/NCAR 40-year reanalysis project. Bull Am Meteor Soc 77:437–471

Kumar A, Zhang L, Wang W (2013) Sea surface temperature-precipitation relationship in different reanalyses. Mon Wea Rev 141:1118–1123

Marsland SJ, Haak H, Jungclaus JH, Latif M, Roeske F (2003) The Max-Planck-Institute global ocean/sea ice model with orthogonal curvilinear coordinates. Ocean Model 5:91–127

Martin GM et al (2011) The HadGEM2 family of Met Office Unified Model climate configurations. Geosci Model Dev 4(723–757):2011

Meehl GA, Washington WM, Arblaster JM, Hu A (2004) Factors affecting climate sensitivity in global coupled models. J Climate 17:1584–1596

Meehl GA, Covey C, Delworth T, Latif M, McAvaney B, Mitchell JFB, Stouffer RJ, Taylor KE (2007) The WCRP CMIP3 multi-model dataset: a new era in climate change research. Bull Am Meteor Soc 88:1383–1394

Mo KC, Kalnay E (1991) Impact of sea surface temperature anomalies on the skill of monthly forecasts. Mon Wea Rev 119:2771–2793

Mo KC, Pfaendtner J, Kalnay E (1987) A GCM study on the maintenance of the June 1982 blocking in the Southern Hemisphere. J Atmos Sci 44:1123–1142

Peña M, Kalnay E, Cai M (2003) Statistics of locally coupled ocean and atmosphere intraseasonal anomalies in Reanalysis and AMIP data. Nonlinear Proc Geoph 10:245–251

Peña M, Cai M, Kalnay E (2004) Life span of subseasonal coupled anomalies. J Climate 17:1597–1604

Raddatz T, Reick C, Knorr W, Kattge J, Roeckner E, Schnur R, Schnitzler KG, Wetzel P, Jungclaus J (2007) Will the tropical land biosphere dominate the climate–carbon cycle feedback during the twenty-first century? Clim Dyn 29:565–574

Rayner NA, Parker DE, Horton EB, Folland CK, Alexander LV, Rowell DP, Kent EC, Kaplan A (2003) Global analyses of sea surface temperature, sea ice, and night marine air temperature since the late nineteenth century. J Geophys Res 108(D14):4407. doi:10.1029/2002JD002670

Reynolds RW, Rayner NA, Smith TM, Stokes DC, Wang W (2002) An improved in situ and satellite SST analysis for climate. J Clim 15:1609–1625

Saha S et al (2010) The NCEP climate forecast system reanalysis. Bull Am Meteor Soc 91:1015–1057

Taylor KE, Stouffer RJ, Meehl GA (2011) An overview of CMIP5 and the experiment design. Bull Am Meteor Soc 93:485–498. doi:10.1175/BAMS-D-11-00094.1

Wang C, Xie S-P, Carton JA (2004) A global survey of ocean–atmosphere interaction and climate variability. In: Wang C et al (eds) Earth's climate: the ocean–atmosphere interaction. Geophysical Monograph Series, V 147, AGU, pp 414

Wang C, Zhenya S, Fangli Q, Shenfu D (2009) What signals are removed and retained by using an anomaly field in climatic research? Int J Oceanogr. doi:10.1155/2009/329754

Xie S-P, Philander SGH (1994) A coupled ocean–atmosphere model of relevance to the ITCZ in the eastern Pacific. Tellus 46A:340–350

Yeager S, Karspeck A, Danabasoglu G, Tribbia J, Teng H (2012) A decadal prediction case study: late twentieth-century North Atlantic Ocean heat content. J Clim 25:5173–5189. doi:10.1175/JCLI-D-11-00595.1

Zhu J, Shukla J (2013) The role of air–sea coupling in seasonal prediction of Asia-Pacific summer monsoon rainfall. J Clim 26:5689–5697. doi:10.1175/JCLI-D-13-00190.1